





# Long-range Ising spins models emerging from frustrated Josephson junctions arrays with topological constraints

Oliver Neyenhuys , Mikhail V. Fistul \*, and Ilya M. Eremin   
*Theoretische Physik III, Ruhr-Universität Bochum, Bochum 44801, Germany*

 (Received 15 August 2023; revised 5 October 2023; accepted 5 October 2023; published 18 October 2023)

Geometrical frustration in correlated systems can give rise to a plethora of ordered states and intriguing phases. Here, we theoretically analyze vertex-sharing frustrated Kagome lattices of Josephson junctions and identify various classical and quantum phases. The frustration is provided by periodically arranged 0- and  $\pi$ -Josephson junctions. In the frustrated regime, the macroscopic phases are composed of different patterns of vortices/antivortices penetrating each basic element of the Kagome lattice, i.e., a superconducting triangle interrupted by three Josephson junctions. We obtain that numerous topological constraints, related to the flux quantization in any hexagon loop, lead to highly anisotropic and long-range interaction between well separated vortices/antivortices. Considering this interaction and a possibility of macroscopic tunneling between vortex and antivortex in single superconducting triangles, we derive an effective Ising-type spin Hamiltonian with strongly anisotropic long-range interaction. In the classically frustrated regime, we numerically calculate the temperature-dependent spatially averaged spin polarization  $\bar{m}(T)$  characterizing the crossover between the ordered and disordered vortex/antivortex states. In the coherent quantum regime, we analyze the lifting of the degeneracy of the ground state and the appearance of the highly entangled states.

DOI: [10.1103/PhysRevB.108.165413](https://doi.org/10.1103/PhysRevB.108.165413)

## I. INTRODUCTION

The collective behavior of the low-energy magnetic excitations crucially depend on the geometry of the lattice they inhabit. For example, antiferromagnetically (AFM) interacting spins on a square lattice form a Néel order with antialigned neighbors. At the same time, their mutual antiparallel alignment cannot be satisfied on a triangular or kagome lattices, which are the most typical models, which feature geometric frustration and yield nontrivial spin order [1–7]. The frustration can also be provided by the competition of interactions of alternating signs of the interactions [1,8], e.g., the ferromagnetic (FM) and AFM ones in addition to a special geometry of the lattices. Typical consequences of the frustration are the highly degenerated ground state, a large amount of low-lying metastable states, and long relaxation times at low temperatures [2,4,9].

Apart from the natural solid-state systems demonstrating a rich plethora of interesting physics behavior due to underlying frustration like that found in iron-based superconductors [10,11], frustrated FM chains [12], kagome magnets [6,13–17], and superconductors [18–21], special attention has been attracted to artificially prepared systems such as trapped ions simulators [22], photonic crystals [23,24], two-dimensional (2D) arrays of Rydberg atoms [25–27], anisotropic optical lattices [28], and Josephson junctions networks [29–34] due to a more efficient way to tune the frustration parameter.

The latter system coined as *frustrated Josephson junction arrays* (f-JJAs) is of special interest since the current

technology allows us to form f-JJAs of various geometries and sizes as well as to tune the frustration by an externally applied magnetic field [30,35,36]. Furthermore, the physics of f-JJAs can be mapped into different nonintegrable quasi-one-dimensional (1D)/2D Ising or  $X$ - $Y$  spins models, and therefore, such arrays can provide a feasible experimental platform to establish analog quantum simulations in the fields of quantum chemistry, quantum biology, and low-dimensional material science [37,38].

It is known that the f-JJAs display nonfrustrated and frustrated regimes characterized by unique and highly degenerated ground states, accordingly. In the frustration regime, plenty of complex ground states such as the checkerboard and ribbon distribution of vortices [29,39] and stripe phases [40], and sharp transitions between these magnetic patterns as the external magnetic field varies, were observed in f-JJAs on square and triangular lattices.

A special type of f-JJA is *vertex-sharing* lattices in which each site is shared between two neighboring triangles, e.g., quasi-1D sawtooth and diamond chains [30,35,41,42] and 2D kagome lattices [7,43]. In the frustration regime of such f-JJAs, the vortex/antivortex penetrates each single superconducting triangle, and various distributions of vortices/antivortices can be realized. The vortex (antivortex) states correspond to anticlockwise (clockwise) persistent currents flowing in a single triangle.

The classical frustrated regime of sawtooth and diamond chains of Josephson junctions has been previously theoretically studied in Ref. [42], where the disordered state of vortices/antivortices was obtained. The lack of ordering in the distribution of vortices/antivortices in such quasi-1D f-JJAs was due to the absence of interaction between vortices/antivortices of different cells. At the same time, for

\*Mikhail.Fistoul@ruhr-uni-bochum.de

f-JJAs based on the kagome lattice, the highly anisotropic distributions of vortices/antivortices forming the ground state have also been predicted [43]. What, however, remains unclear is what type of interaction can lead to the formation of such ordered anisotropic patterns and how the order-disorder phase transition in vortex patterns occurs. Moreover, at low temperatures, one can expect due to charging effects an intriguing interplay between the quantum superposition of classical vortex/antivortex states and the interaction of well-separated vortices/antivortices.

In this paper, we address these questions performing a systematic theoretical study of classical and coherent quantum collective states occurring in an exemplary 2D vertex-sharing frustrated kagome lattice of Josephson junctions. In a complete analogy with the magnetic systems where FM and AFM couplings coexist, we introduce the frustration as a periodic alternation of 0- and  $\pi$ -Josephson junctions. The  $\pi$ -Josephson junctions can be fabricated on a basis of various multijunction SQUIDS in an externally applied magnetic field [29,30,32–34,44–46], superconductor-FM-superconductor junctions [47], different facets of grain boundaries of high-temperature superconductors [48], or Josephson junctions between two-band superconductors [49]. By making use of this model, we show explicitly that, in the frustration regime, the vortices/antivortices penetrate a basic element of the kagome lattice, i.e., a superconducting triangle interrupted by three (two-0 and one- $\pi$ ) Josephson junctions. The observed collective states of vortices/antivortices are determined by numerous topological constraints related to the flux quantization in any hexagon loop leading to an effective interaction between vortices/antivortices of different triangles.

This paper is organized as follows: In Sec. II, we present the electrodynamic model and the general approach allowing one to quantitatively analyze collective classical and quantum states arising in the kagome lattice of frustrated Josephson junctions with numerous topological constraints occurring in such arrays. In Sec. III, we study the low-lying states of a single building block of vertex-sharing f-JJAs, i.e., three  $\pi/0$ -Josephson junctions incorporated in a single superconducting loop. In the frustrated regime, we arrive at a single spin model in which two basis spin states correspond to (counter)clockwise persistent currents or the penetration of the vortex/antivortex. In Sec. IV, our analysis is extended to the kagome lattice of frustrated Josephson junctions for which we derive an effective (2D + 1) Ising spin model with a long-ranged and spatially anisotropic interaction between well-separated spins. In Secs. V and VI, we analyze the classical and coherent quantum frustrated regimes and the corresponding phases. Section VII provides conclusions. The details of the calculation of the partition function of interacting spins  $Z$  and an explicit spatial dependence of the interaction strength in the infinite kagome lattice will be presented in Appendices A and B, respectively.

## II. MODEL, GENERAL APPROACH, AND TOPOLOGICAL CONSTRAINTS

We consider a vertex-sharing 2D kagome lattice of superconducting nodes (islands) in which the adjacent nodes are connected by Josephson junctions as schematically shown

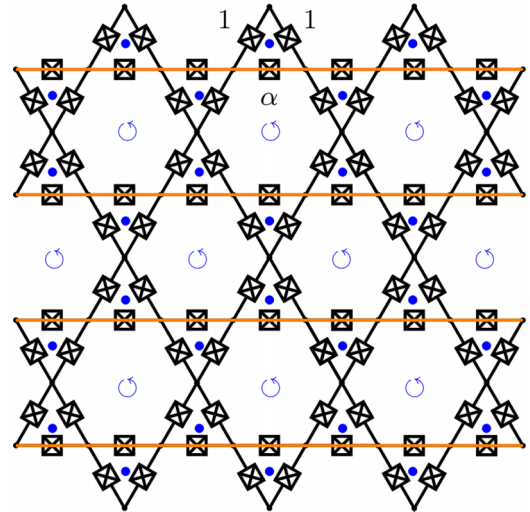


FIG. 1. Schematics of the frustrated kagome lattice of Josephson junctions. The  $\pi$ - and the 0-Josephson junctions are indicated by orange and black lines, respectively. Two kinds of closed loops, i.e., the triangles (blue dots) and hexagons (blue circles), are shown.

in Fig. 1. The frustration is induced by the special periodic arrangement of 0- and  $\pi$ -Josephson junctions. The Josephson junction connecting the superconducting  $i$  and  $j$  nodes is characterized by two physical parameters: the Josephson coupling energy  $\alpha_{ij}E_J$  and the charging energy  $E_C/|\alpha_{ij}|$ , where  $E_J = \hbar I_c/(2e)$  and  $E_C = e^2/(2C)$  are determined by the critical current  $I_c$  and the capacitance  $C$ , respectively. The parameters  $\alpha_{ij}$  were chosen as  $\alpha_{ij} = \alpha$  for all horizontal links (orange lines in Fig. 1) and  $\alpha_{ij} = 1$  for all other links. The parameter  $\alpha$  is then varied as  $-1 \leq \alpha \leq 1$ , and therefore,  $\alpha > 0$  ( $\alpha < 0$ ) defines 0 ( $\pi$ )-Josephson junctions. The parameter  $\alpha$  also relates to the commonly introduced frustration parameter  $f$  as  $f = (1 - \alpha)/2$ , which varies between 0 and 1.

The classical dynamics of Josephson junctions arrays is determined by the time-dependent Josephson phases  $\varphi_{ij}(t)$ . The partition function  $Z$  can be expressed via the path integral in the imaginary time-representation:

$$Z = \int \exp\left(-\frac{S_E}{\hbar}\right) \mathcal{D}[\varphi_{ij}(\tau)], \quad (1)$$

where the Euclidean action is given by

$$S_E = \int_0^{\hbar/(k_B T)} \mathcal{L}\{\varphi_{ij}, \dot{\varphi}_{ij}, i\tau\} d\tau, \quad (2)$$

and the Euclidean Lagrangian  $\mathcal{L}$  of a Josephson junction array is written as

$$\mathcal{L} = \sum_{\langle ij \rangle} \frac{|\alpha_{ij}| \hbar^2}{8E_C} [\dot{\varphi}_{ij}]^2 + \alpha_{ij} E_J (1 - \cos \varphi_{ij}). \quad (3)$$

Here,  $\langle ij \rangle$  refers to the two nearest-neighbor nodes coupled by a Josephson junction. Note, the measure  $\mathcal{D}[\varphi_{ij}(\tau)]$  considers that the Josephson phases  $\varphi_{ij}(\tau)$  are not independent and must satisfy numerous topological constraints. They originate from the fact that the flux quantization, i.e., the sum of the  $\varphi_{ij}$  along any closed loop of the lattice, must be  $2\pi n$ , where  $n$  is an integer. These constraints are considered explicitly in Eq. (1)

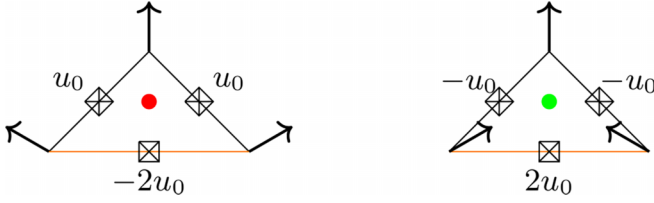


FIG. 2. Schematics of a single superconducting triangle loop interrupted by three Josephson junctions. In the frustrated regime [ $\alpha < \alpha_c$  ( $f > f_c$ )], the classical ground state is doubly degenerate. The penetrating (anti)vortices are shown by (green)red circles. Corresponding Josephson phases are indicated.

as

$$Z = \int \exp\left(-\frac{S_E}{\hbar}\right) \left\{ \prod_l \delta[C_l(\varphi_{pk}) - 2\pi n] \right\} \prod_{(ij)} d\varphi_{ij}, \quad (4)$$

with

$$C_\ell(\varphi_{pk}) = \sum_{(pk) \in \text{closed loop}, \ell} \varphi_{pk},$$

and  $\ell$  is the constraint number.

### III. BUILDING BLOCK OF f-JJAS: FRUSTRATED REGIME

As a starting point of our analysis, we now derive the effective Euclidean Lagrangian of a building block of the kagome lattice: a single superconducting triangle interrupted by three Josephson junctions, as shown in Fig. 2. Such a system is characterized by three Josephson phases  $\varphi_{1-3}(\tau)$ , which must satisfy a single constraint  $\varphi_1 + \varphi_2 + \varphi_3 = 0$ . The corresponding Euclidean Lagrangian of a superconducting triangle then depends on two degrees of freedom  $\varphi_{1,2}$ , as

$$\begin{aligned} \mathcal{L}^\Delta = & \frac{\hbar^2}{8E_C} [\dot{\varphi}_1 \quad \dot{\varphi}_2] \begin{bmatrix} 1 + |\alpha| & |\alpha| \\ |\alpha| & 1 + |\alpha| \end{bmatrix} \begin{bmatrix} \dot{\varphi}_1 \\ \dot{\varphi}_2 \end{bmatrix} \\ & + E_J [2 + \alpha - \cos(\varphi_1) - \cos(\varphi_2) - \alpha \cos(\varphi_1 + \varphi_2)]. \end{aligned} \quad (5)$$

Introducing symmetric and antisymmetric variables  $\varphi_s = (\varphi_1 + \varphi_2)/2$  and  $\varphi_a = (\varphi_2 - \varphi_1)/2$ , one can obtain the extrema of the potential energy. If  $\alpha < \alpha_c = -0.5$  ( $f > f_c = \frac{3}{4}$ ), the potential energy has two equivalent minima as  $\varphi_s = \pm u_0$ , with  $u_0 = \arccos(\frac{1}{2|\alpha|})$ , and  $\varphi_a = 0$ . These minima are separated by the potential barrier of the height  $E_J(\alpha) = E_J[2(1 + \alpha) + 1/(2\alpha)]$ , which becomes zero at the critical value of  $\alpha = \alpha_c$ . Thus, the classical ground state is doubly degenerate (frustrated) and corresponds to the counterclockwise (a vortex) or clockwise (an antivortex) persistent currents (see Fig. 2). Notice here that the frustrated regime is completely equivalent to the states of a flux qubit at the symmetry point [44,45].

Restricting ourselves to a study of low-lying excitations, we now use the following approximations. First, we neglect high-frequency oscillations of the asymmetric Josephson phase  $\varphi_a$ . Second, the exact dependence of the potential energy on  $\varphi_s$  [Eq. (5)] is approximated by harmonic potentials around the two classical minima. The effective classical spin

degree of freedom  $\sigma = \pm 1$  is introduced to distinguish between the vortex/antivortex states. Then the Lagrangian of a single superconducting triangle is written as

$$\mathcal{L}^\Delta = \frac{\hbar^2 \gamma}{4E_C} \dot{\varphi}_s^2 + \frac{E_J(\alpha)}{u_0^2} [\varphi_s(\tau) - u_0 \sigma(\tau)]^2, \quad (6)$$

where  $\gamma = 1 + 2|\alpha|$ . Such a reduced Lagrangian depends on two degrees of freedom: the Josephson phase  $\varphi_s(\tau)$  and the spin values  $\sigma(\tau)$ . Since the Lagrangian in Eq. (6) depends quadratically on  $\varphi_s(\tau)$ , one can integrate out this degree of freedom and obtain the *effective spin model*. Indeed, for a single triangle, the partition function  $Z^\Delta\{\sigma(\tau)\}$  is calculated by expanding  $\varphi_s(\tau)$  and  $\sigma(\tau)$  in the sum over the Matsubara frequencies  $\omega_m = 2\pi k(k_B T)/\hbar$ , where  $k = 0, \pm 1, \dots$ , i.e.,

$$\varphi_s(\tau) = \sum_{\omega_k} \tilde{\varphi}(\omega_k) \exp(i\omega_k \tau), \quad (7)$$

and

$$\sigma(\tau) = \sum_{\omega_k} \tilde{\sigma}(\omega_k) \exp(i\omega_k \tau). \quad (8)$$

Integrating over all  $\tilde{\varphi}(\omega_k)$ , we obtain

$$Z^\Delta\{\tilde{\sigma}(\omega_k)\} \propto \exp \left[ \frac{E_J(\alpha)}{k_B T} \sum_{\omega_k} \frac{\Omega^2}{\omega_k^2 + \Omega^2} |\tilde{\sigma}(\omega_k)|^2 \right], \quad (9)$$

where the characteristic frequency  $\Omega$  of small oscillations of  $\varphi_s$  is  $\Omega = [2/(\hbar u_0)] \sqrt{E_C E_J(\alpha)/\gamma}$ .

### IV. EFFECTIVE ISING SPIN HAMILTONIAN

Next, we extend our analysis from a single superconducting triangle to the kagome lattice. It is convenient to present the kagome lattice as a periodic repetition in two directions  $\ell$  and  $m$  of the tuple  $(\ell m)$ . Each tuple is a rhombus with the sides connecting hexagon loop centers, and it contains two triangles: downward (+) and upward (-) pointing. Such a representation of the kagome lattice is presented in Fig. 3.

A single superconducting triangle belonging to the tuple  $(\ell m)$  is characterized by two imaginary time-dependent degrees of freedom  $\varphi_{\ell m \pm}(\tau)$  and  $\sigma_{\ell m \pm}(\tau)$ , and the Euclidean Lagrangian is

$$\mathcal{L} = \sum_{\ell m \pm} \mathcal{L}^\Delta[\varphi_{\ell m \pm}, \dot{\varphi}_{\ell m \pm}, \sigma_{\ell m \pm}], \quad (10)$$

where the Lagrangian of a single superconducting triangle  $\mathcal{L}^\Delta$  is determined by Eq. (6).

This Lagrangian must be accompanied by the topological constraints  $C_{\ell m} = 2\pi n$  related to the flux quantization in the hexagon loop  $(\ell m)$ . Notice that, if  $\alpha$  is not equal to specific values  $-1; -(1/\sqrt{2})$ , one can use the constraints with  $n = 0$  only. The expression of  $C_{\ell m}$  depends on the Josephson phases  $\varphi_{ij \pm}$  of triangles surrounding the hexagon loop  $(\ell m)$  (see Fig. 4). It is written as

$$C_{\ell m}(\tau) = \sum_{ij} \varphi_{ij \pm}(\tau) G_{ij \pm, \ell m}, \quad (11)$$

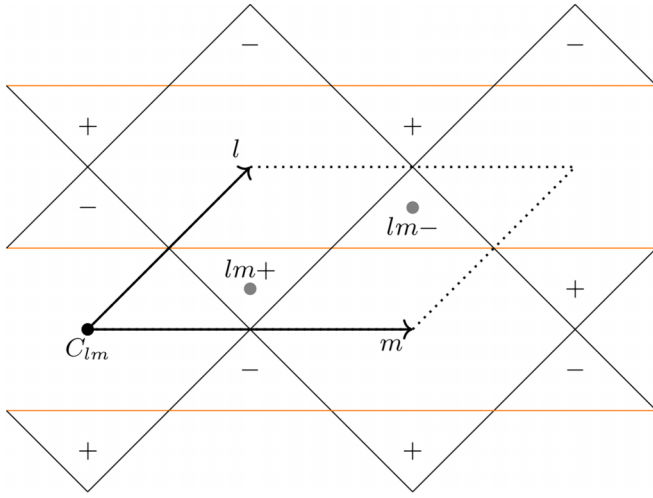


FIG. 3. Representation of the kagome lattice as the two-dimensional (2D) periodic lattice of tuples. Each tuple  $(l, m)$  labels a rhombus with sides connecting the nearest hexagon loops centers and contains downward-pointing (+) and upward-pointing (-) triangles.

where

$$\begin{aligned} G_{ij+;\ell m} &= -2\delta_{ij;[(\ell-1)m]} + \delta_{ij;[\ell(m-1)]} + \delta_{ij;[\ell m]}, \\ G_{ij-;\ell m} &= -2\delta_{ij;[\ell(m-1)]} + \delta_{ij;[(\ell-1)m]} + \delta_{ij;[(\ell-1)(m-1)]}. \end{aligned} \quad (12)$$

Here,  $\delta_{ij;[\ell m]}$  is the Kronecker symbol.

By making use of the identity:

$$\delta[C_{\ell m}(\tau)] = \int \mathcal{D}[p_{\ell m}(\tau)] \exp \left[ -\frac{i}{\hbar} \int_0^{\hbar/(k_B T)} p_{\ell m} C_{\ell m} d\tau \right], \quad (13)$$

Eq. (4) for the partition function  $Z$  is written as

$$\begin{aligned} Z &\propto \int \mathcal{D}[\varphi_{ij\pm}(\tau)] \mathcal{D}[p_{\ell m}(\tau)] \\ &\times \exp \left\{ -\frac{1}{\hbar} \int_0^{\hbar/(k_B T)} \left[ \mathcal{L} + i \sum_{\ell m} p_{\ell m} C_{\ell m} \right] d\tau \right\}. \end{aligned} \quad (14)$$

Substituting Eqs.(10) and (11) into Eq. (14) and performing all integrals over  $\varphi_{\ell m\pm}(\omega_k)$  and  $\tilde{p}_{\ell m}(\omega_k)$  (details of straightfor-

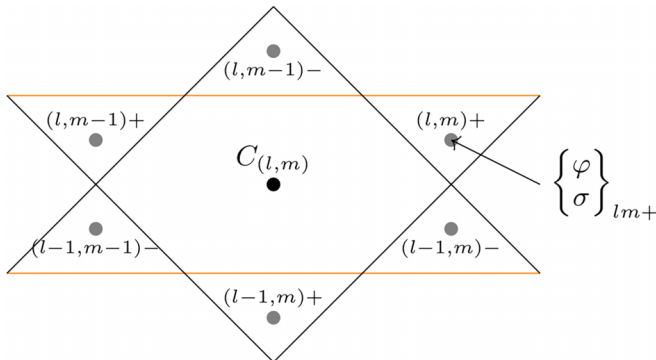


FIG. 4. Topological constraint  $C_{lm} = 0$  for a single hexagon loop. The Josephson phase  $\varphi_{\ell, m}$  and spin degree of freedom  $\sigma$  are shown.

ward but tedious calculations are presented in Appendix A), we obtain the partition function  $Z\{\tilde{\sigma}_{\ell m\pm}(\omega_k)\}$  of the interacting spin model as follows:

$$Z\{\tilde{\sigma}_{\ell m\pm}(\omega_k)\} \propto \exp \left( -\frac{E_J(\alpha)}{k_B T} \sum_{\omega_k} \frac{\Omega^2}{\omega_k^2 + \Omega^2} [\mathcal{F}_0 + \mathcal{F}_{\text{int}}] \right), \quad (15)$$

where the the spatially local term  $\mathcal{F}_0$  is expressed as

$$\mathcal{F}_0 = - \sum_{\ell m;\pm} |\tilde{\sigma}_{\ell m\pm}(\omega_k)|^2, \quad (16)$$

and the interaction term  $\mathcal{F}_{\text{int}}$  is written as

$$\begin{aligned} \mathcal{F}_{\text{int}} &= \sum_{\ell m} \sum_{ij} [\tilde{\sigma}_{ij\pm}(\omega_k) G_{ij,\ell m}^{\pm\pm} \tilde{\sigma}_{\ell m\pm}(-\omega_k) \\ &\quad + \tilde{\sigma}_{ij\mp}(\omega_k) G_{ij,\ell m}^{\mp\pm} \tilde{\sigma}_{\ell m\pm}(\omega_k)]. \end{aligned} \quad (17)$$

Here, we introduce the coupling strengths between the spins  $\sigma$  of different triangles:

$$G_{ij,\ell m}^{\pm\pm} = G_{ij\pm,tu} (G_+^\dagger G_+ + G_-^\dagger G_-)^{-1}_{tu,vv} G_{vv,\ell m\pm}^\dagger, \quad (18)$$

and

$$G_{ij,\ell m}^{\mp\pm} = G_{ij\mp,tu} (G_+^\dagger G_+ + G_-^\dagger G_-)^{-1}_{tu,vv} G_{vv,\ell m\pm}^\dagger. \quad (19)$$

Observe that, in all terms of Eqs. (17)–(19), the upper (lower) indices were chosen.

To conclude this section, we notice that the partition function  $Z$  of the effective Ising spin model contains two contributions: quantum fluctuations of spins  $\sigma$  of individual triangles and the interaction between spins of different triangles.

## V. CLASSICAL FRUSTRATED REGIME

Here, we present an analysis of the partition function  $Z$  and corresponding collective spin (vortices/antivortices) phases in the classically frustrated regime  $k_B T \gg \hbar\Omega$ . In this limit, the main contribution to the sum over  $\omega_k$  in Eq. (15) comes from  $\omega_k = 0$ , and we obtain the classical 2D Ising model of interacting spins with the partition function:

$$Z^{\text{cl}}\{\sigma_{\ell m\pm}\} \propto \exp \left[ -\frac{E_J(\alpha)}{k_B T} \mathcal{F}_{\text{int}}^{\text{cl}}\{\sigma_{\ell m\pm}\} \right], \quad (20)$$

where the Ising-type interaction is given by

$$\mathcal{F}_{\text{int}}^{\text{cl}} = \sum_{\ell m} \sum_{ij} [\sigma_{ij\mp} G_{ij,\ell m}^{\mp\pm} \sigma_{\ell m\pm} + \sigma_{ij\pm} G_{ij,\ell m}^{\pm\pm} \sigma_{\ell m\pm}]. \quad (21)$$

One finds that, in the classical frustrated regime, the observed spin patterns are determined by a single parameter  $E_J(\alpha)/k_B T$ , and one can identify two distinguished regimes. The first one is realized in the high-temperature limit  $k_B T \gg E_J(\alpha)$ , in which all distributions of spins have the same probabilities, and we have a disordered spin configuration. In the low-temperature regime  $k_B T \ll E_J(\alpha)$ , the spin patterns demonstrate a specific ordering determined by the anisotropic and long-ranged interaction strength  $\mathcal{F}_{\text{int}}^{\text{cl}}$ .

To quantitatively characterize the order-disorder phase transition for the kagome lattice of a small size, we

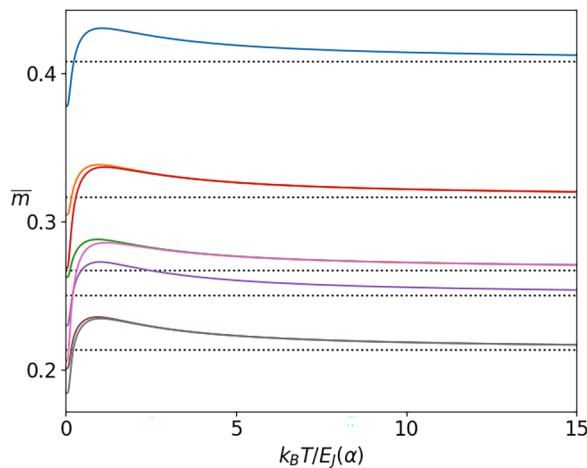


FIG. 5. Calculated temperature dependence of  $\bar{m}(T)$  for the kagome lattice containing a few plaquettes (from up to bottom): 1,  $1 \times 2$  ( $2 \times 1$ ),  $2 \times 2$ , and  $3 \times 2$  ( $2 \times 3$ ) are shown. The dotted lines indicate the values of  $\bar{m} = 1/\sqrt{N}$  in the limit of infinite temperature.

counted all spin configurations and obtained the temperature dependence of a spatially averaged spin polarization  $\bar{m}(T) = \sqrt{\langle M^2 \rangle}$ , where  $\langle M^2 \rangle = \sum_M P_M M^2$ , and  $M = (1/N)(\sum_{ij;\pm} \sigma_{ij;\pm})$ . Here,  $P_M$  is the probability of a spin pattern with the spin polarization  $M$ , and it is determined by the partition function  $Z^{cl}$ . Also,  $N$  is the total number of triangles. The obtained dependencies of  $\bar{m}(T)$  for the kagome lattice of different sizes  $N$  are presented in the Fig. 5. All curves show the maximum for  $k_B T / E_J(\alpha) \simeq 1$ , indicating the crossover between the ordered and disordered spin phases.

Since in the high-temperature limit  $P_{M=2n-N} \simeq C_n^N / 2^N$ , where  $n$  is the number of triangles with the spin  $\sigma = +1$ , we obtain  $\bar{m}(T) = 1/\sqrt{N}$  (see dotted lines in Fig. 5). In the low-temperature limit, as shown in Ref. [43], the spin patterns become highly anisotropic, and their number drastically reduces from  $2^N$  to  $2^{\sqrt{N}}$ . Moreover, only a few spin patterns give nonzero contribution to the spin polarization  $m$ , and the value of  $\bar{m}$  reduces substantially with  $N$  in this limit (see Fig. 5). As we turn to the large-sized kagome lattice, the interaction strength between spins shows highly anisotropic behavior. The interaction term  $G^{\pm\pm}$  becomes a spatially local one and does not contribute to the classical partition function in Eq. (20). The interaction strengths  $G^{\mp\pm}$  are written as (the details of calculations are presented in Appendix B)

$$\begin{aligned} G_{\ell m; \ell' m'}^{+-} |_{m-m'=\ell'-\ell-1} &= -\frac{1}{2} \frac{1}{2^{|\ell'-\ell|}}, \\ G_{\ell m; \ell' m'}^{+-} |_{m-m'=0} &= -\frac{1}{2} \frac{1}{2^{|\ell-\ell'|}}, \\ G_{\ell m; \ell' m'}^{+-} |_{m-m' \approx (\ell-\ell')/2} &\propto \frac{2\sqrt{2}}{(|\ell-\ell'|)^{1/2} \sqrt{\pi}}. \end{aligned} \quad (22)$$

The 2D color plot of  $G_{\vec{p}\vec{p}'}^{+-(-)}$  as presented in Fig. 6 shows both algebraic and exponential decay of the interaction strengths in vertical and horizontal directions. Moreover, the interaction  $G_{00;\ell m}^{+-}$  ( $G_{\ell m;00}^{+-}$ ) is absent in the upper (lower) part of the lattice.

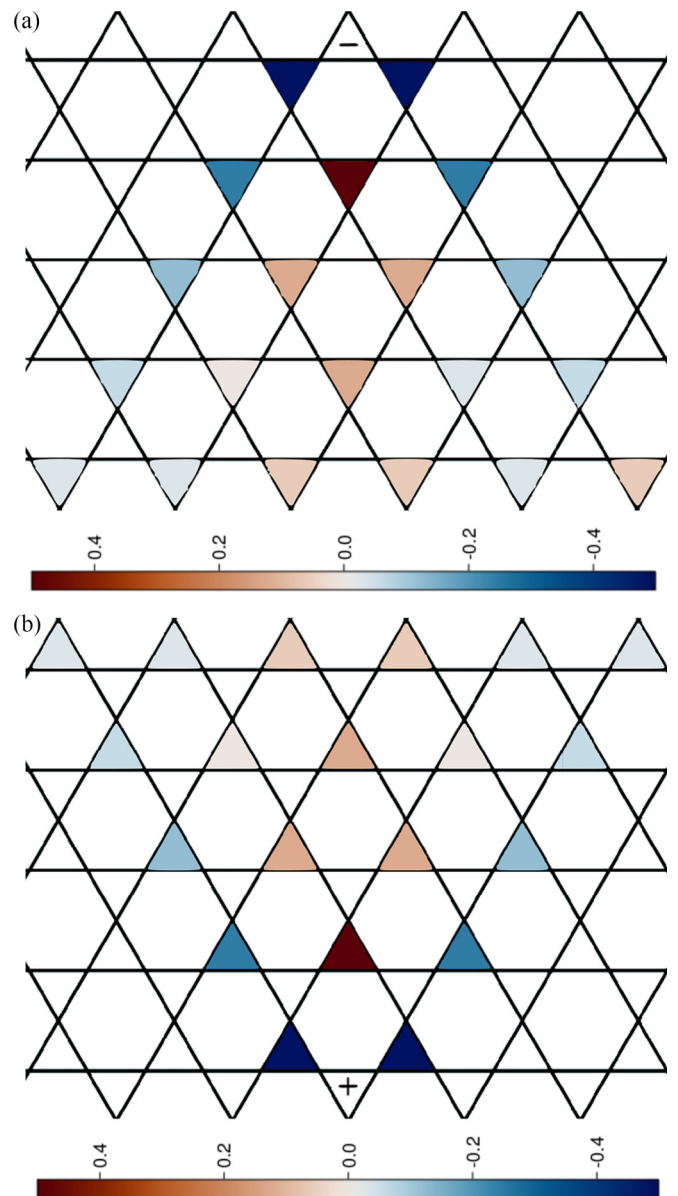


FIG. 6. Calculated two-dimensional color plot of the interaction strength: (a)  $G_{00;\ell m}^{+-}$  and (b)  $G_{\ell m;00}^{+-}$ , where the downward-pointing (+) and upward-pointing (-) triangles (00) are indicated.

To observe the thermodynamic phase transition, we perform classical Monte Carlo numerical simulations of the  $30 \times 30$  frustrated kagome lattices of Josephson junctions based on the partition function in Eqs. (20) and (21) employing open boundary conditions. In all simulations, we started from the disordered (high-temperature) state and cooled to temperature  $T$ . With this procedure, we obtain the transition from the disordered vortex/antivortex patterns at  $k_B T / E_J(\alpha) \geq 0.2$  to the stripe-type AFM order for  $k_B T / E_J(\alpha) \leq 0.19$  and below where the ordering is FM along the  $x$  direction and AFM along the  $y$  direction with the period of the stripe of  $\sim 11$  coupled vertex-shared triangles. It is presented in Fig. 7. Interestingly enough, the stripe-type AFM order sets in despite of the long-range frustrated interaction along the  $y$  direction and initial 14-fold degeneracy

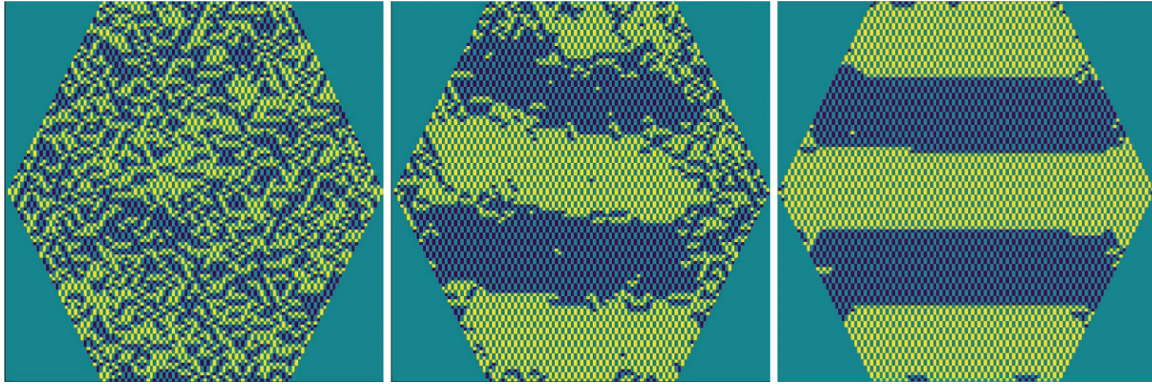


FIG. 7. Calculated typical vortex/antivortex patterns obtained in large  $30 \times 30$  frustrated kagome lattices of Josephson junctions using open boundary conditions for different temperatures:  $k_B T / E_J(\alpha) = 0.2$  (left);  $k_B T / E_J(\alpha) = 0.19$  (middle); and  $k_B T / E_J(\alpha) = 0.12$  (right). Quenching from the high-temperature disordered state was used. Dark blue (yellow) rectangles correspond to the vortex (antivortex) shared by two vertex-shared triangles (see Fig. 4). Light blue rectangles are empty spots.

of the ground state for a single kagome plaquette. At low temperatures, we also observed more complex patterns with long domain walls stretched along other symmetry axes (not shown).

## VI. THE COHERENT QUANTUM REGIME

In the limit  $k_B T \ll \hbar\Omega$ , the quantum fluctuations and therefore nonzero Matsubara frequencies in Eq. (15) start to play an important role. Calculating the sum over the Matsubara frequencies in Eq. (15), we obtain that a spatially local term  $\propto \mathcal{F}_0$  produces the interaction in the imaginary time domain as  $\sigma(\tau_i)\sigma(\tau_j)$ , where  $|\tau_i - \tau_j| \simeq 1/\Omega$ . For  $E_J(\alpha) \gg \hbar\Omega$ , this interaction yields small-amplitude quantum tunneling between the vortex and antivortex of single triangles. The spatially nonlocal terms in Eq. (15) lead to the strong Ising type of interaction described by Eq. (21). Putting all terms together, we obtain the total Hamiltonian in this regime:

$$\hat{H} = \hat{H}_{\text{loc}} + \hat{H}_{\text{int}}, \quad (23)$$

where

$$\hat{H}_{\text{loc}} = \sum_{\ell m; \pm} \Delta \hat{\sigma}_{\ell m; \pm}^x, \quad (24)$$

and

$$\hat{H}_{\text{int}} = E_J(\alpha) \hat{\mathcal{F}}_{\text{int}}^{\text{cl}} \{ \hat{\sigma}_{\ell m; \pm}^z; \hat{\sigma}_{ij; \pm}^z \}, \quad (25)$$

where  $\hat{\mathcal{F}}_{\text{int}}^{\text{cl}}$  is described by Eq. (21), and the tunneling amplitude is  $\Delta \simeq \hbar\Omega \exp[-2E_J/(\hbar\Omega)]$ . Thus, the low-temperature quantum regime is described by Eq. (23), which corresponds to the seminal model of interacting Ising spins in the transverse magnetic field.

The quantum dynamics of such a model is determined by two parameters:  $\Delta$  and  $E_J(\alpha)$ . Carrying out the direct numerical diagonalization, we obtain the eigenvalues and eigenfunctions of all quantum states in a single plaquette of the kagome lattice as a function of the ratio  $E_J/\Delta$ . Such a dependence of the normalized eigenspectrum  $E/\sqrt{E_J^2 + \Delta^2}$  is presented in Fig. 8. In the absence of the interaction  $E_J(\alpha) \ll \Delta$ , the quantum ground state of each superconducting triangle

is the symmetric quantum superposition of vortex and antivortex states. The ground state of a whole plaquette is the direct product of these states, i.e., the symmetric quantum superposition of all 64 classical vortex/antivortex states, and the quantum entanglement is absent in this regime. Notice also that this regime that can be realized as the parameter  $\alpha$  is in close vicinity to the critical value  $\alpha = -\frac{1}{2}$ .

However, the most interesting case occurs as the tunneling amplitude  $\Delta$  is much smaller than the interaction strength  $E_J(\alpha)$ . In this limit, the eigenspectrum is split into the well-defined bands, as shown in Fig. 9, for the parameter  $\Delta = E_J/20$ . The lowest band contains different quantum superpositions of the 14-fold degenerate classical ground state presented explicitly in Ref. [43].

Furthermore, we obtain that, if in the classical regime the ground state is 14-fold degenerate (blue points in Fig. 9), even a tiny amplitude of the quantum tunneling  $\Delta$  results in the lifting of this classical degeneracy and the corresponding energy distribution among different spin patterns (yellow points in Fig. 9). Moreover, in the quantum regime, the wave functions

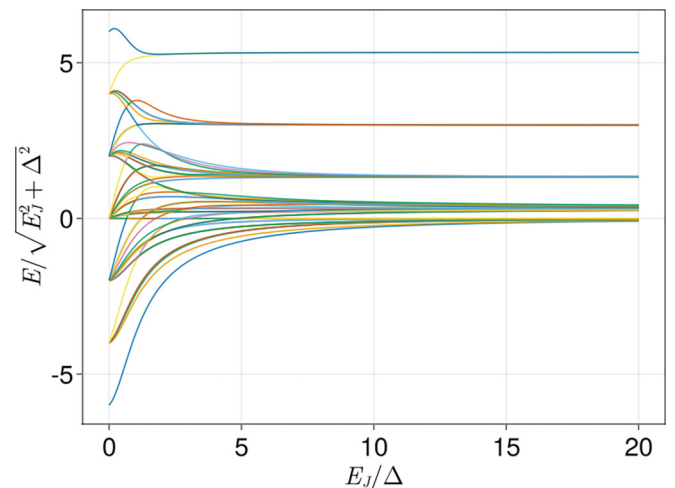


FIG. 8. Calculated energy spectrum as a function of dimensionless parameter  $E_J(\alpha)/\Delta$ .

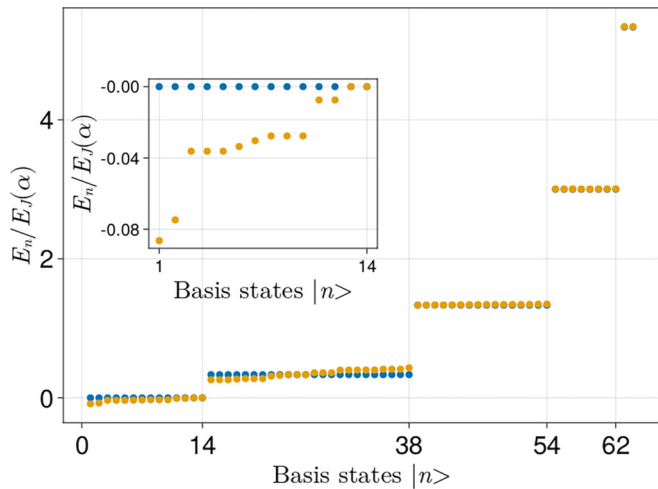


FIG. 9. Calculated energy distribution of different spin patterns for a single plaquette of the kagome lattice: The classical and coherent quantum regimes are shown by the blue and yellow points, respectively. An enlarged area of 14 low-lying eigenstates is shown in the inset. The tunneling parameter  $\Delta = E_J(\alpha)/20$  was used.

$\Psi$  of the ground and excited states are formed as a highly entangled combination of basis (classical) spin patterns  $|n\rangle$ . The obtained corresponding matrix elements  $f_n = \langle \Psi | n \rangle$  and probabilities  $|f_n|^2$  are shown in Figs. 10 and 11. One sees that the maximum contribution to the quantum ground and first excited states comes from the 12 (two highly symmetric vortex/antivortex patterns are excluded) vortex/antivortex patterns forming the classical ground state.

To conclude this section, we notice that the analysis of spatiotemporal correlations of the quantum ground state of the Hamiltonian in Eqs. (23)–(25) in large kagome lattices of Josephson junctions requires using special methods going

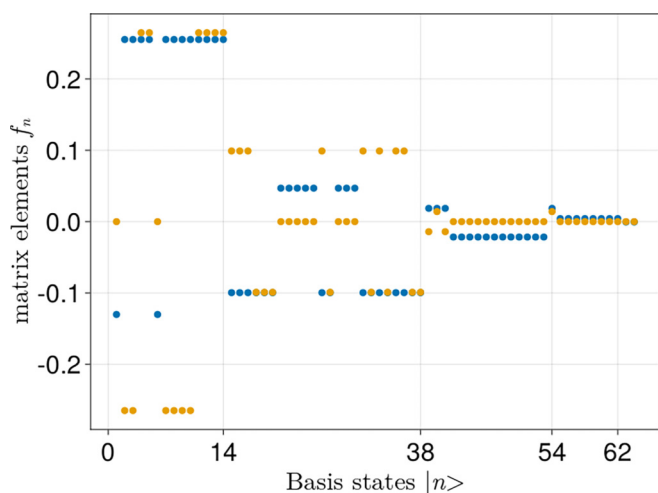


FIG. 10. Calculated wave functions of the ground state (blue points) and the first excited state (yellow points) represented by their matrix elements to the basis states  $|n\rangle$  of the classical spin-interacting Hamiltonian  $\hat{H}^{cl}$ . The tunneling parameter  $\Delta = E_J(\alpha)/20$  was chosen.

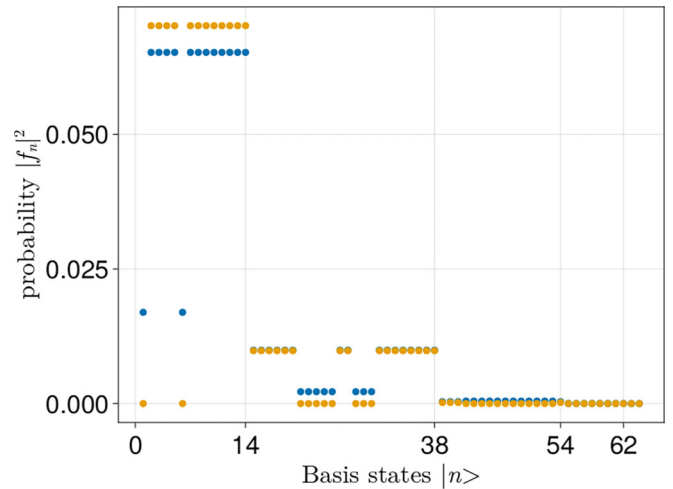


FIG. 11. Calculated ground (blue points) and first excited (yellow points) states represented by their probabilities of the basis states  $|n\rangle$  of the classical spin-interacting Hamiltonian  $\hat{H}^{cl}$ . The tunneling parameter is  $\Delta = E_J(\alpha)/20$ .

beyond direct numerical diagonalization and will be presented elsewhere.

### VII. CONCLUSIONS

To conclude, we theoretically analyzed the classical and quantum phases occurring in a frustrated vertex-sharing 2D kagome lattice of Josephson junctions where the frustration is provided by a periodic arrangement of 0- and  $\pi$ -Josephson junctions. The frustrated regime is characterized by a highly degenerated ground state once the frustration parameter  $f$  exceeds the critical value  $f_c = \frac{3}{4}$ . In this regime, the (counter)clockwise persistent current flows into a single building block of the kagome lattice, i.e., a superconducting triangle interrupted by three Josephson junctions (Fig. 2). These persistent currents are characterized by classical spin values of  $\sigma = \pm 1$ .

The quantitative analysis of different patterns of persistent currents (vortices/antivortices) occurring in the kagome lattice of Josephson junctions is made by the exact mapping of the initial model of an f-JJA onto the effective Ising Hamiltonian of interacting spins. The presence of numerous topological constraints related to the flux quantization in any hexagon loop of the kagome lattice results in long- and short-ranged highly anisotropic interactions between well-separated spins. For the kagome lattices of large size, the interaction shows a weak algebraic decay along the vertical axis and exponential decay along the horizontal axis [Fig. 6 and Eq. (22)], absent of a nonlocal interaction between spins of the same pointing triangles. The spatial anisotropy of the vortex/antivortex phases obtained at  $T = 0$  [43] is naturally explained by the anisotropy of the interaction  $G^{+-(-+)}$ .

In the classically frustrated regime  $k_B T \gg \hbar \Omega$ , we obtained the order-disorder phase transition (crossover due to a finite-sized system) in the patterns of persistent currents. Such a crossover is presented in Fig. 5 as the temperature-dependent spin polarization  $m(T)$  for the kagome lattice composed of a

few plaquettes. For kagome lattices of large size, we obtain the disordered vortex/antivortex patterns at high temperatures and stripe-type AFM order at low temperatures (see, Fig. 7).

In the quantum regime, we obtain that the macroscopic tunneling between vortices and antivortices in a single superconducting triangle lifts the degeneracy of the classical ground state and, in the absence of interaction, yields the symmetric quantum superposition of all 64 classical states in a single plaquette of the kagome lattice (see Fig. 8). Such a quantum ground state demonstrates zero entanglement. However, as the topological constraint-induced interaction is large, i.e.,  $E_J(\alpha) \gg \Delta$ , even a tiny amplitude of the quantum tunneling  $\Delta$  results in the quantum ground state composed of the highly

entangled combination of basis (classical) persistent current patterns (see Figs. 9–11).

Finally, we notice that f-JJAs arranged in vertex-sharing 2D lattices can be used as an ideal physical platform to establish the quantum modeling of generic Ising spin models with constraints [50] to obtain various collective states in magnetic, optical, and superconducting systems.

### ACKNOWLEDGMENTS

We acknowledge the financial support through the European Union's Horizon 2020 research and innovation program under Grant Agreement No. 863313 'Supergalax'. We thank Alexei Andreanov for fruitful discussions.

### APPENDIX A: DERIVATION OF THE PARTITION FUNCTION OF THE EFFECTIVE ISING MODEL OF INTERACTING SPINS

We start from Eq. (14) for the partition function, considering the topological constraints and the Lagrangians of single triangles:

$$Z \propto \int \mathcal{D}[\varphi_{ij\pm}(\tau)] \mathcal{D}[p_{\ell m}(\tau)] \exp \left\{ -\frac{1}{\hbar} \int_0^{\hbar/(k_B T)} \left[ \sum_{\ell m \pm} \frac{\hbar^2 \gamma}{4E_C} \dot{\varphi}_{\ell m \pm}^2 + \frac{E_J(\alpha)}{u_0^2} [\varphi_{\ell m \pm}(\tau) - u_0 \sigma_{\ell m \pm}(\tau)]^2 + i \sum_{\ell m} p_{\ell m} \sum_{ij \pm} \varphi_{ij(\tau) \pm} G_{ij \pm; \ell m} \right] d\tau \right\}. \quad (\text{A1})$$

Introducing  $M = \hbar^2 \gamma / 2E_C$ , exchanging the indices in the second summation, and expanding the quadratic term, the partition function can be expressed as

$$Z \propto \int \mathcal{D}[\varphi_{ij\pm}(\tau)] \mathcal{D}[p_{\ell m}(\tau)] \exp \left\{ -\frac{M}{2\hbar} \int_0^{\hbar/(k_B T)} \left[ \sum_{\ell m \pm} \dot{\varphi}_{\ell m \pm}^2 + \Omega^2 (\varphi_{\ell m \pm}^2 + u_0^2) + \varphi_{\ell m \pm} \left( -2u_0 \Omega^2 \sigma_{\ell m \pm} + i \frac{2}{M} \sum_{ij} p_{ij} G_{\ell m \pm; ij} \right) \right] d\tau \right\}. \quad (\text{A2})$$

In the next step, we switch to the Matsubara representation:

$$Z \propto \int \mathcal{D}[\tilde{\varphi}_{ij\pm}(\omega_k)] \mathcal{D}[\tilde{p}_{\ell m}(\omega_k)] \exp \left( -\frac{M}{2k_B T} \sum_{\omega_k} \left\{ \sum_{\ell m \pm} (\omega_k^2 + \Omega^2) \tilde{\varphi}_{\ell m \pm}(\omega_{-k}) \tilde{\varphi}_{\ell m \pm}(\omega_k) + 2\tilde{\varphi}_{\ell m \pm}(\omega_{-k}) \times \left[ -u_0 \Omega^2 \tilde{\sigma}_{\ell m \pm}(\omega_k) + i \frac{1}{M} \sum_{ij} \tilde{p}_{ij}(\omega_k) G_{\ell m \pm; ij} \right] \right\} d\tau \right), \quad (\text{A3})$$

and notice that we have a quadratic form in every  $\tilde{\varphi}_{\ell m \pm}(\omega_k)$ . Integrating out the quadratic form, we are left with

$$Z \propto \int \mathcal{D}[\tilde{p}_{\ell m}(\omega_k)] \exp \left\{ -\frac{M}{2k_B T} \sum_{\omega_k} \left[ \sum_{\ell m \pm} -\frac{u_0^2 \Omega^4}{(\omega_k^2 + \Omega^2)} \tilde{\sigma}_{\ell m \pm}(\omega_{-k}) \tilde{\sigma}_{\ell m \pm}(\omega_k) + \frac{\sum_{ijqr} \tilde{p}_{qr}(\omega_{-k}) G_{qr; \ell m \pm}^\dagger G_{\ell m \pm; ij} \tilde{p}_{ij}(\omega_k)}{M^2 (\omega_k^2 + \Omega^2)} - \Omega^2 u_0^2 \delta_{k0} + i \frac{u_0 \Omega^2}{M (\omega_k^2 + \Omega^2)} \sum_{ij} \tilde{\sigma}_{\ell m \pm}(\omega_{-k}) G_{\ell m \pm; ij} \tilde{p}_{ij}(\omega_k) + i \frac{u_0 \Omega^2}{M (\omega_k^2 + \Omega^2)} \sum_{ij} \tilde{p}_{ij}(\omega_{-k}) G_{ij; \ell m \pm}^\dagger \tilde{\sigma}_{\ell m \pm}(\omega_k) \right] \right\}. \quad (\text{A4})$$

Next, we obtain a quadratic form in the constraint fields  $\tilde{p}_{\ell m}(\omega_k)$ . For that, we write the constraint fields and spins as vectors with indexed lattice number ( $\ell m$ ). We thus introduce the vectors  $\vec{p}$ ,  $\vec{\sigma}_+$ , and  $\vec{\sigma}_-$  as well as the matrices  $G_+$  and  $G_-$ . The partition



function can then be written as

$$Z \propto \int \mathcal{D}[\vec{p}(\omega_k)] \exp \left\{ -\frac{M}{2k_B T} \sum_{\omega_k} \left[ \sum_{\pm} -\frac{u_0^2 \Omega^4}{(\omega_k^2 + \Omega^2)} \vec{\sigma}_{\pm}(\omega_{-k}) \cdot \vec{\sigma}_{\pm}(\omega_k) + \frac{\vec{p}^T(\omega_{-k})(G_+^\dagger G_+ + G_-^\dagger G_-) \vec{p}(\omega_k)}{M^2(\omega_k^2 + \Omega^2)} \right. \right. \\ \left. \left. + i \frac{u_0 \Omega^2}{M(\omega_k^2 + \Omega^2)} \vec{\sigma}_{\pm}^T(\omega_{-k}) G_{\pm} \vec{p}(\omega_k) + i \frac{u_0 \Omega^2}{M(\omega_k^2 + \Omega^2)} \vec{p}^T(\omega_{-k}) G_{\pm}^\dagger \vec{\sigma}_{\pm}(\omega_k) \right] \right\}. \quad (\text{A5})$$

Integrating out the quadratic form over  $\vec{p}$ , we obtain the final expression:

$$Z \propto \exp \left\{ -\frac{M u_0^2 \Omega^2}{2k_B T} \sum_{\omega_k} \frac{\Omega^2}{(\omega_k^2 + \Omega^2)} \sum_{\pm} \left[ -\vec{\sigma}_{\pm}(\omega_{-k}) \cdot \vec{\sigma}_{\pm}(\omega_k) + \vec{\sigma}_{\pm}^T(\omega_{-k}) G_{\pm} (G_+^\dagger G_+ + G_-^\dagger G_-)^{-1} G_{\pm}^\dagger \vec{\sigma}_{\pm}(\omega_k) \right. \right. \\ \left. \left. + \vec{\sigma}_{\mp}^T(\omega_{-k}) G_{\mp} (G_+^\dagger G_+ + G_-^\dagger G_-)^{-1} G_{\mp}^\dagger \vec{\sigma}_{\pm}(\omega_k) \right] \right\}. \quad (\text{A6})$$

Realizing that  $M u_0^2 \Omega^2 / 2 = E_J(\alpha)$  and going back from the vector notation to indexed notation, we arrive at Eq. (15) of the main text.

## APPENDIX B: THE ISING SPIN-SPIN INTERACTION IN THE INFINITE KAGOME LATTICE

For a spatially infinite kagome lattice, one can diagonalize the constraint-dependent interaction matrices  $G$  by the Fourier transformation on the lattice:

$$\tilde{\varphi}_{lm\pm}(\omega_k) = \frac{1}{(2\pi)^2} \int_{q=-\pi}^{\pi} \int_{r=-\pi}^{\pi} dq dr z_{qr\pm}(\omega_k) \exp[i(lq + mr)], \quad (\text{B1})$$

$$\tilde{p}_{lm}(\omega_k) = \frac{1}{(2\pi)^2} \int_{q=-\pi}^{\pi} \int_{r=-\pi}^{\pi} dq dr \pi_{qr}(\omega_k) \exp[i(lq + mr)], \quad (\text{B2})$$

$$\tilde{\sigma}_{lm\pm}(\omega_k) = \frac{1}{(2\pi)^2} \int_{q=-\pi}^{\pi} \int_{r=-\pi}^{\pi} dq dr \Sigma_{qr\pm}(\omega_k) \exp[i(lq + mr)]. \quad (\text{B3})$$

With these constraints defined in Eq. (12), we obtain expressions for the entries of the diagonalized constraint matrices in the Fourier space:

$$\mathcal{G}_{qr+} = 1 + e^{ir} - 2e^{iq} \quad (\text{B4})$$

$$\mathcal{G}_{qr-} = \exp[i(r + q)] + e^{iq} - 2e^{ir}, \quad (\text{B5})$$

and the modulus of the entries does not depend on the sign index  $\pm$ :

$$|\mathcal{G}_{qr}|^2 = \mathcal{G}_{qr\pm}^* \mathcal{G}_{qr\pm} = -4 \sin^2\left(\frac{r}{2}\right) + 8 \sin^2\left(\frac{q-r}{2}\right) + 8 \sin^2\left(\frac{q}{2}\right). \quad (\text{B6})$$

Since the matrices are diagonal, we can easily calculate their inverse and express the interaction matrices in Eqs. (18) and (19) as

$$G_{lm'l'm'}^{\pm\pm} = \frac{1}{(2\pi)^2} \iint_{-\pi}^{\pi} \frac{\mathcal{G}_{qr\pm} \mathcal{G}_{qr\pm}^*}{2|\mathcal{G}_{qr}|^2} \exp\{-i[q(l-l') + r(m-m')]\} dr dq \\ = \frac{1}{(2\pi)^2} \iint_{-\pi}^{\pi} \frac{1}{2} \exp\{-i[q(l-l') + r(m-m')]\} dr dq = \frac{1}{2} \delta_{ll'} \delta_{mm'}, \quad (\text{B7})$$

and

$$G_{lm'l'm'}^{\pm\mp} = G_{l'm'l'm}^{\mp\pm} \frac{1}{2(2\pi)^2} \iint_{-\pi}^{\pi} \frac{\mathcal{G}_{qr\pm} \mathcal{G}_{qr\mp}^*}{2|\mathcal{G}_{qr}|^2} \exp\{-i[q(l-l') + r(m-m')]\} dr dq \\ = \frac{1}{(2\pi)^2} \iint_{-\pi}^{\pi} \frac{1 + e^{ir} - 2e^{iq}}{\exp[i(q+r)] + e^{iq} - 2e^{ir}} \exp\{-i[q(l-l') + r(m-m')]\} dr dq. \quad (\text{B8})$$

As one can see from Eq. (B7), the interaction between different spins within one sublattice vanishes in the infinite system. We are thus left with interactions between the sublattices given by Eq. (B8). To evaluate the integral, we perform the substitution

$z_r = e^{ir}$  and  $z_q = e^{iq}$  and obtain

$$\begin{aligned}
 2(2\pi)^2 G_{lm'l'm'}^{\pm\mp} &= 2(2\pi)^2 G_{l'm'l'm}^{\mp\pm} \\
 &= - \oint_{S_1} \oint_{S_1} \frac{z_r^{-1} z_q^{-1} + z_q^{-1} - 2z_r^{-1}}{z_r z_q + z_q - 2z_r} z_q^{-(l-l')} z_r^{-(m-m')} dz_r dz_q \\
 &= - \oint_{S_1} \oint_{S_1} \frac{1}{z_r z_q + z_q - 2z_r} z_q^{-(l-l'+1)} z_r^{-(m-m'+1)} dz_r dz_q - \oint_{S_1} \oint_{S_1} \frac{1}{z_r z_q + z_q - 2z_r} z_q^{-(l-l'+1)} z_r^{-(m-m')} dz_r dz_q \\
 &\quad + \oint_{S_1} \oint_{S_1} \frac{2}{z_r z_q + z_q - 2z_r} z_q^{-(l-l')} z_r^{-(m-m'+1)} dz_r dz_q \\
 &= [1] + [2] + [3],
 \end{aligned} \tag{B9}$$

where we labeled the last three integrals as [1], [2], [3]. First, we perform the integration over  $z_q$  and then over  $z_r$ . By virtue of the residue theorem, we can compute the integral by evaluating the residue of the poles within the unit circle. We start by investigating the function  $f_n(z_q)$ :

$$f_n(z_q) = \frac{1}{z_r z_q + z_q - 2z_r} z_q^{-n}. \tag{B10}$$

There are only two poles for  $z_q$ : the poles at  $z_{q0} = 0$  and  $z_{q1} = 2z_r / (1 + z_r)$ . Since  $|z_q| > 1$  for almost all  $z_r \in S_1$ , its contribution will vanish when performing the integral over  $z_r$ . Thus, it is sufficient to calculate the residue at  $z_{q0}$  only:

$$\begin{aligned}
 \text{Res}(f_n, 0) &= \frac{1}{(n-1)!} \lim_{z_q \rightarrow 0} \frac{d^{n-1}}{dz_q^{n-1}} \frac{1}{z_r z_q + z_q - 2z_r} \\
 &= \frac{1}{(n-1)!} \lim_{z_q \rightarrow 0} \frac{(n-1)! (-1)^{n-1} (z_r + 1)^{n-1}}{(z_r z_q + z_q - 2z_r)^n} \\
 &= \frac{(-1)^{n-1} (z_r + 1)^{n-1}}{(-2z_r)^n} = \frac{-(z_r + 1)^{n-1}}{2^n z_r^n}.
 \end{aligned} \tag{B11}$$

To perform integration over  $z_r$ , we will take a look at the function  $g_{nh}(z_r)$ :

$$g_{nh}(z_r) = (z_r + 1)^h z_r^{-n}. \tag{B12}$$

In the case of  $h \geq 0$ , we are only left with the residue at  $z_{r0} = 0$ :

$$\begin{aligned}
 \text{Res}(g, 0) &= \frac{1}{(n-1)!} \lim_{z_r \rightarrow 0} \frac{d^{n-1}}{dz_r^{n-1}} (z_r + 1)^h \\
 &= \frac{1}{(n-1)!} \lim_{z_r \rightarrow 0} (z_r + 1)^{h-(n-1)} \frac{h!}{[h-(n-1)]!} \\
 &= \binom{h}{n-1} \Big|_{h \geq n-1}.
 \end{aligned} \tag{B13}$$

With this in mind, we can finally evaluate our interlattice interaction:

$$\begin{aligned}
 G_{lm'l'm'}^{\pm\mp} &= G_{l'm'l'm}^{\mp\pm} \\
 &= -\frac{1}{2} \frac{1}{2^{l-l'}} \binom{l-l'}{l-l'+m-m'+1} \Big|_{|l-l' \geq 0; -1 \geq m-m' \geq l-l-1} - \frac{1}{2} \frac{1}{2^{l-l'}} \binom{l-l'}{m-m'+l-l'} \Big|_{|l-l' \geq 0; 0 \geq m-m' \geq l-l} \\
 &\quad + 2 \frac{1}{2^{l-l'}} \binom{l-l'-1}{m-m'+l-l'} \Big|_{|l-l' \geq 1; -1 \geq m-m' \geq l-l}.
 \end{aligned} \tag{B14}$$

- [1] P. W. Anderson, The concept of frustration in spin glasses, *J. Less Common Met.* **62**, 291 (1978).  
 [2] R. Moessner and A. P. Ramirez, Geometrical frustration, *Phys. Today* **59**, 24 (2006).

- [3] C. Schröder, H. Nojiri, J. Schnack, P. Hage, M. Luban, and P. Kögerler, Competing spin phases in geometrically frustrated magnetic molecules, *Phys. Rev. Lett.* **94**, 017205 (2005).

- [4] L. Balents, Spin liquids in frustrated magnets, *Nature (London)* **464**, 199 (2010).
- [5] A. Baniodeh, N. Magnani, Y. Lan, G. Buth, C. E. Anson, J. Richter, M. Affronte, J. Schnack, and A. K. Powell, High spin cycles: Topping the spin record for a single molecule verging on quantum criticality, *npj Quantum Mater.* **3**, 10 (2018).
- [6] T.-H. Han, J. S. Helton, S. Chu, D. G. Nocera, J. A. Rodriguez-Rivera, C. Broholm, and Y. S. Lee, Fractionalized excitations in the spin-liquid state of a kagome-lattice antiferromagnet, *Nature (London)* **492**, 406 (2012).
- [7] F.-F. Song and G.-M. Zhang, Tensor network approach to the fully frustrated XY model on a kagome lattice with a fractional vortex-antivortex pairing transition, *Phys. Rev. B* **108**, 014424 (2023).
- [8] C. Nisoli, R. Moessner, and P. Schiffer, *Colloquium*: Artificial spin ice: Designing and imaging magnetic frustration, *Rev. Mod. Phys.* **85**, 1473 (2013).
- [9] S. Mahmoudian, L. Rademaker, A. Ralko, S. Fratini, and V. Dobrosavljević, Glassy dynamics in geometrically frustrated Coulomb liquids without disorder, *Phys. Rev. Lett.* **115**, 025701 (2015).
- [10] S.-S. Gong, W. Zhu, D. N. Sheng, and K. Yang, Possible nematic spin liquid in spin-1 antiferromagnetic system on the square lattice: Implications for the nematic paramagnetic state of FeSe, *Phys. Rev. B* **95**, 205132 (2017).
- [11] R. M. Fernandes, A. V. Chubukov, and J. Schmalian, What drives nematic order in iron-based superconductors? *Nat. Phys.* **10**, 97 (2014).
- [12] M. E. Zhitomirsky and H. Tsunetsugu, Magnon pairing in quantum spin nematic, *Europhys. Lett.* **92**, 37001 (2010).
- [13] S. Yan, D. A. Huse, and S. R. White, Spin-liquid ground state of the  $s = \frac{1}{2}$  kagome Heisenberg antiferromagnet, *Science* **332**, 1173 (2011).
- [14] M. G. Yamada, T. Soejima, N. Tsuji, D. Hirai, M. Dincă, and H. Aoki, First-principles design of a half-filled flat band of the kagome lattice in two-dimensional metal-organic frameworks, *Phys. Rev. B* **94**, 081102(R) (2016).
- [15] L. Messio, B. Bernu, and C. Lhuillier, Kagome antiferromagnet: A chiral topological spin liquid? *Phys. Rev. Lett.* **108**, 207204 (2012).
- [16] M. Fujihala, K. Morita, R. Mole, S. Mitsuda, T. Tohyama, S. ichiro Yano, D. Yu, S. Sota, T. Kuwai, A. Koda *et al.*, Gapless spin liquid in a square-kagome lattice antiferromagnet, *Nat. Commun.* **11**, 3429 (2020).
- [17] X. Teng, J. S. Oh, H. Tan, L. Chen, J. Huang, B. Gao, J.-X. Yin, J.-H. Chu, M. Hashimoto, D. Lu *et al.*, Magnetism and charge density wave order in kagome FeGe, *Nat. Phys.* **19**, 814 (2023).
- [18] T. Neupert, M. M. Denner, J.-X. Yin, R. Thomale, and M. Z. Hasan, Charge order and superconductivity in kagome materials, *Nat. Phys.* **18**, 137 (2022).
- [19] X. Feng, K. Jiang, Z. Wang, and J. Hu, Chiral flux phase in the kagome superconductor  $AV_3Sb_4$ , *Sci. Bull.* **66**, 1384 (2021).
- [20] J.-X. Yin, B. Lian, and M. Z. Hasan, Topological kagome magnets and superconductors, *Nature (London)* **612**, 647 (2022).
- [21] J. Yang, X. Yi, Z. Zhao, Y. Xie, T. Miao, H. Luo, H. Chen, B. Liang, W. Zhu, Y. Ye *et al.*, Observation of flat band, Dirac nodal lines and topological surface states in kagome superconductor  $CsTi_3Bi_5$ , *Nat. Commun.* **14**, 4089 (2023).
- [22] J. W. Britton, B. C. Sawyer, A. C. Keith, C.-C. J. Wang, J. K. Freericks, H. Uys, M. J. Biercuk, and J. J. Bollinger, Engineered two-dimensional Ising interactions in a trapped-ion quantum simulator with hundreds of spins, *Nature (London)* **484**, 489 (2012).
- [23] S. Weimann, L. Morales-Inostroza, B. Real, C. Cantillano, A. Szameit, and R. A. Vicencio, Transport in sawtooth photonic lattices, *Opt. Lett.* **41**, 2414 (2016).
- [24] R. A. Vicencio, C. Cantillano, L. Morales-Inostroza, B. Real, C. Mejía-Cortés, S. Weimann, A. Szameit, and M. I. Molina, Observation of localized states in Lieb photonic lattices, *Phys. Rev. Lett.* **114**, 245503 (2015).
- [25] G. Semeghini, H. Levine, A. Keesling, S. Ebadi, T. T. Wang, D. Bluvstein, R. Verresen, H. Pichler, M. Kalinowski, R. Samajdar *et al.*, Probing topological spin liquids on a programmable quantum simulator, *Science* **374**, 1242 (2021).
- [26] G. Giudici, M. D. Lukin, and H. Pichler, Dynamical preparation of quantum spin liquids in Rydberg atom arrays, *Phys. Rev. Lett.* **129**, 090401 (2022).
- [27] Z. Yan, Y.-C. Wang, R. Samajdar, S. Sachdev, and Z. Y. Meng, Emergent glassy behavior in a kagome Rydberg atom array, *Phys. Rev. Lett.* **130**, 206501 (2023).
- [28] M. Xu, L. H. Kendrick, A. Kale, Y. Gang, G. Ji, R. T. Scalettar, M. Lebrat, and M. Greiner, Frustration- and doping-induced magnetism in a Fermi-Hubbard simulator, *Nature (London)* **620**, 971 (2023).
- [29] M. S. Rzchowski, Phase transitions in a kagomé lattice of Josephson junctions, *Phys. Rev. B* **55**, 11745 (1997).
- [30] I. M. Pop, K. Hasselbach, O. Buisson, W. Guichard, B. Pannetier, and I. Protopopov, Measurement of the current-phase relation in Josephson junction rhombi chains, *Phys. Rev. B* **78**, 104504 (2008).
- [31] J. Q. You, X.-F. Shi, X. Hu, and F. Nori, Quantum emulation of a spin system with topologically protected ground states using superconducting quantum circuits, *Phys. Rev. B* **81**, 014505 (2010).
- [32] M. W. Johnson, M. H. Amin, S. Gildert, T. Lanting, F. Hamze, N. Dickson, R. Harris, A. J. Berkley, J. Johansson, P. Bunyk *et al.*, Quantum annealing with manufactured spins, *Nature (London)* **473**, 194 (2011).
- [33] A. D. King, J. Carrasquilla, J. Raymond, I. Ozfidan, E. Andriyash, A. Berkley, M. Reis, T. Lanting, R. Harris, F. Altomare *et al.*, Observation of topological phenomena in a programmable lattice of 1,800 qubits, *Nature (London)* **560**, 456 (2018).
- [34] A. D. King, J. Raymond, T. Lanting, S. V. Isakov, M. Mohseni, G. Poulin-Lamarre, S. Ejtemaee, W. Bernoudy, I. Ozfidan, A. Y. Smirnov *et al.*, Scaling advantage over path-integral Monte Carlo in quantum simulation of geometrically frustrated magnets, *Nat. Commun.* **12**, 1113 (2021).
- [35] B. Douçot and J. Vidal, Pairing of Cooper pairs in a fully frustrated Josephson-junction chain, *Phys. Rev. Lett.* **88**, 227005 (2002).
- [36] V. Cataudella and R. Fazio, Glassy dynamics of Josephson arrays on a dice lattice, *Europhys. Lett.* **61**, 341 (2003).
- [37] A. J. Daley, I. Bloch, C. Kokail, S. Flannigan, N. Pearson, M. Troyer, and P. Zoller, Practical quantum advantage in quantum simulation, *Nature (London)* **607**, 667 (2022).
- [38] I. Buluta and F. Nori, Quantum simulators, *Science* **326**, 108 (2009).

- [39] P. Caputo, M. V. Fistul, and A. V. Ustinov, Resonances in one and two rows of triangular Josephson junction cells, *Phys. Rev. B* **63**, 214510 (2001).
- [40] D. Valdez-Balderas and D. Stroud, Superconductivity versus phase separation, stripes, and checkerboard ordering: A two-dimensional Monte Carlo study, *Phys. Rev. B* **72**, 214501 (2005).
- [41] M. Rizzi, V. Cataudella, and R. Fazio,  $4e$ -condensation in a fully frustrated Josephson junction diamond chain, *Phys. Rev. B* **73**, 100502(R) (2006).
- [42] A. Andrianov and M. V. Fistul, Resonant frequencies and spatial correlations in frustrated arrays of Josephson type nonlinear oscillators, *J. Phys. A: Math. Theor.* **52**, 105101 (2019).
- [43] A. Andrianov and M. V. Fistul, Frustration-induced highly anisotropic magnetic patterns in the classical XY model on the kagome lattice, *Phys. Rev. B* **102**, 140405(R) (2020).
- [44] T. P. Orlando, J. E. Mooij, L. Tian, C. H. van der Wal, L. S. Levitov, S. Lloyd, and J. J. Mazo, Superconducting persistent-current qubit, *Phys. Rev. B* **60**, 15398 (1999).
- [45] P. Jung, S. Butz, M. Marthaler, M. V. Fistul, J. Leppäkangas, V. P. Koshelets, and A. V. Ustinov, Multistability and switching in a superconducting metamaterial, *Nat. Commun.* **5**, 3730 (2014).
- [46] K. V. Shulga, E. Il'ichev, M. V. Fistul, I. S. Besedin, S. Butz, O. V. Astafiev, U. Hübner, and A. V. Ustinov, Magnetically induced transparency of a quantum metamaterial composed of twin flux qubits, *Nat. Commun.* **9**, 150 (2018).
- [47] A. K. Feofanov, V. A. Oboznov, V. V. Bol'ginov, J. Lisenfeld, S. Poletto, V. V. Ryazanov, A. N. Rossolenko, M. Khabipov, D. Balashov, A. B. Zorin *et al.*, Implementation of superconductor/ferromagnet/superconductor  $\pi$ -shifters in superconducting digital and quantum circuits, *Nat. Phys.* **6**, 593 (2010).
- [48] H. Hilgenkamp, Pi-phase shift Josephson structures, *Supercond. Sci. Technol.* **21**, 034011 (2008).
- [49] R. G. Dias and A. M. Marques, Frustrated multiband superconductivity, *Supercond. Sci. Technol.* **24**, 085009 (2011).
- [50] A. Lucas, Ising formulations of many NP problems, *Front. Phys.* **2**, 5 (2014).